Biogeochemistry (2010) 98:9–27
DOI 10.1007/s10533-009-9372-2

ORIGINAL PAPER

Chemical weathering and solute export by meltwater in a maritime Antarctic glacier basin

Andy Hodson · Tim Heaton · Harry Langford · Kevin Newsham

Received: 4 December 2008 / Accepted: 1 September 2009 / Published online: 22 September 2009

Abstract Solute yields, laboratory dissolution data and both chemical and isotopic markers of rock weathering reactions are used to characterise the biogeochemistry of glacial meltwaters draining a maritime Antarctic glacier. We find that delayed flowpaths through ice-marginal talus and moraine sediments are critical for the acquisition of solute from rock minerals because delayed flowpaths through subglacial sediments are absent beneath this small, cold-based glacier. Here the mechanisms of weathering are similar to those reported in subglacial environments, and include sub-oxic conditions in the early summer and increasingly oxic conditions thereafter. Up to 85% of the NO_3^- and 65% of the SO_4^{2-} are most likely produced by bacterially mediated reactions in these ice marginal sediments. However, reactive pyrite phases are sparse in the host rocks, limiting the export of Fe, SO_4^{2-} and cations that may be removed by weathering once pyrite oxidation has taken place. This means that dissolution of Ca^{2+} and Na^+ from carbonate and silicate minerals dominate, producing moderate cationic denudation yields from Tuva Glacier (163 Σ*meq$^+$ m^{-2} a^{-1}) compared to a global range of values (94–4,200 Σ*meq$^+$ km^{-2} a^{-1}). Overall, crustally derived cations represent 42% of the total cationic flux, the rest being accounted for by snowpack sources.

Keywords Antarctica · Chemical denudation · Glacial meltwater · Rock–water interaction

A. Hodson (✉) · H. Langford
Department of Geography, University of Sheffield, Sheffield S10 2TN, UK
e-mail: a.j.hodson@sheffield.ac.uk

T. Heaton
NERC Isotope Geosciences Laboratory, British Geological Survey, Keyworth, Nottingham, UK

K. Newsham
British Antarctic Survey, High Cross, Madingley Road, Cambridge, UK

Introduction

Studies of the composition of runoff from Antarctica are very sparse, a limitation that is only partly justified by the fact that this is the coldest, driest continent on Earth. Logistical difficulties are also very significant and so we have a far from complete understanding of the biogeochemical processes that are activated following melt. To date, the biogeochemistry of lakes is far better understood than runoff: both from a process perspective and from a geographical one (see Vincent et al. 2008). Most research attention has been given to the geochemistry of Victoria Land (e.g. Borghini and Bargagli 2004; De Mora et al. 1991) and in particular its McMurdo Dry Valleys (e.g. Green et al. 1988; Nezat et al. 2001; Lyons et al. 2003; McKnight et al. 2008 and references therein). The

remote, dry location of these valleys means that discontinuous flowpaths and sporadic runoff events dominate. The low levels of precipitation also mean that runoff from glacial meltwaters is most important, and a number of papers have described their biogeochemistry as a result (e.g., Fortner et al. 2005). Once such runoff leaves the glacier, there is a significant effect from biogeochemical cycling within the hyporheic zone, where evaporation leads to the formation and subsequent dissolution of secondary salts (Gooseff et al. 2002; Nezat et al. 2001).

Virtually nothing is known about the geochemistry of runoff from the Antarctic Peninsula and its islands. Here one has to rely upon studies of lake inflow waters and occasional spatial sampling campaigns to acquire a rudimentary understanding of the processes that operate (e.g. Caulkett and Ellis-Evans 1997; Hodgson et al., in press). We believe this is a significant research limitation because it is here that climate warming is forcing extremely rapid responses from ecosystems at the ice margin (Quayle et al. 2002). Nutrient provision from snowmelt, ground thaw, rock–water interaction and marine fauna appear to have a marked effect upon nutrient availability following melt (Quayle et al. 2002; Hodson 2006). The climate is also more conducive to condensation than evaporation, so that the production of secondary minerals is more likely to be due to the incongruent dissolution of primary minerals than evaporite formation.

More data sets from the Antarctic Peninsula are urgently required if the coupling between climate change and biogeochemical cycling is to be understood here. The purpose of this paper is therefore to help address this need by examining solute acquisition following rock–water contact in a small glacial catchment upon Signy Island of the South Orkney Island group. A combination of geochemical and stable isotope tracers are employed to characterise the capacity of glacial runoff to acquire new nutrients from crustal sources, and thus fertilise marine ecosystems known for their Fe-limitation (Watson et al. 2000). The efficacy of chemical denudation will also be assessed through comparison with a global glacial data set.

Field site

Research was undertaken in a small glacier basin (unofficial name: Tuva Glacier) that forms an outlet of the Signy Island ice cap in the maritime Antarctic (South Orkney Islands; Fig. 1). The catchment ranges from sea level to ca. 250 m altitude, is composed of meta-sedimentary rocks (mostly schists but with some marble and amphibolites; see Mathews and Maling 1967) and is 1.01 km^2 in area (to Site Q1, installed at ca. 50 m altitude). The glacier is almost certainly cold-based and offers no rock–water contact at the glacier bed. Snowmelt therefore supplies runoff to high rock–water contact zones in the talus and moraines that flank the valley sides. Snow and glacier melt almost entirely runs off via the southwest margin, much of which is routed through a small lake next to the end moraine on its way to Site Q2. Otherwise, a very small stream (<10% of total glacial runoff) drains along northern margin of the glacier. Runoff from all parts of the forefield also contributes to the proglacial stream between Sites Q2 and Q1 downstream. Here flow through a series of icings and then boulder-filled channels takes place. More details of the hydrological dynamics in the system are available from Hodson (2006), who provides a water balance. This indicated an annual specific runoff of 0.53 m a^{-1} for the water year under study (2003/04), demonstrating the significance of the melting that takes place in this part of Antarctica.

Samples were collected for chemical and isotopic measurements from across the catchment between Day Of Year (DOY) 317, 2003 and DOY 81, 2004. This interval encompassed the entire runoff season, although isotope samples could not be collected after DOY 8, 2004. The stable isotopic data therefore describe an early low flow phase of the runoff season, allowing the particular emphasis to be given to the first stages of rock–water-organism interaction following snowmelt.

Methods

Hydrochemical sampling

A comprehensive programme of snow, ice, bulk deposition, snow melt and runoff sampling was undertaken and has already been described by Hodson (2006). However, here we report new data from zones of high rock–water contact and present the stable isotopic composition of all sample types for the first time. Figure 1 shows the location of these

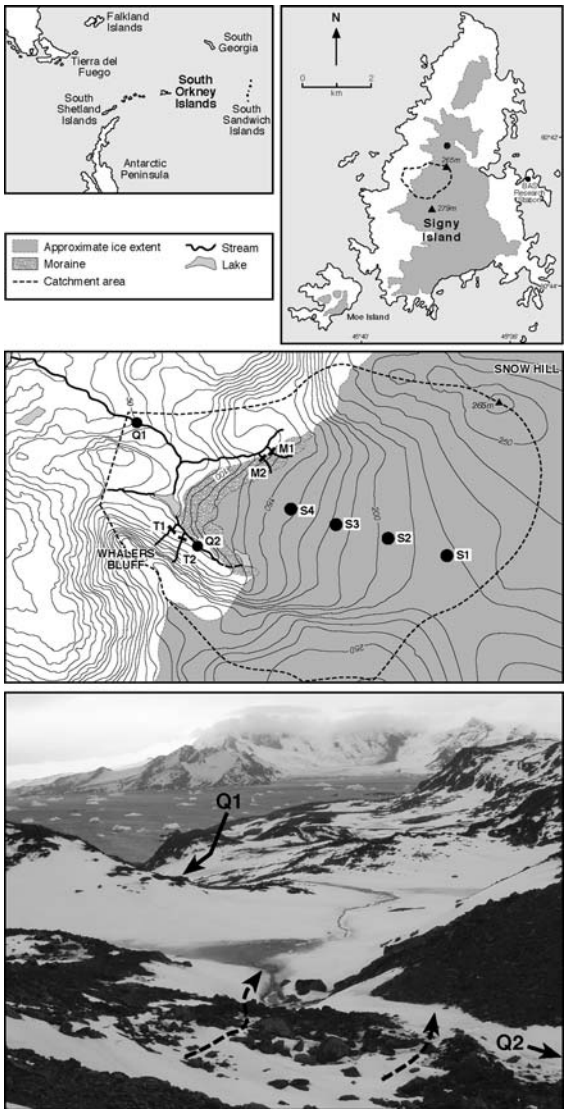

Fig. 1 The study area and sampling sites. T1 and T2 are talus waters, whilst M1 and M2 are moraine waters. The river draining the catchment was sampled at sites Q1 and Q2. S1–S4 are snow pits. *Photographic inset*: view of lower catchment taken from T1 and looking towards the north west. The *hatched line* shows the T1 and T2 flowpaths, whilst the *solid arrows* indicate the location of Q1 and Q2 monitoring sites

sites. Bulk snow samples that were taken for chemical and stable isotopic characterisation were collected from four pits down the glacier centre line (S1 to S4 in Fig. 1) between DOYs 317 and 333, 2003 (prior to runoff) and stored in pre-cleaned plastic bags prior to melting in a water bath and filtration through a 0.45 μm high capacity Gelman filter. Proglacial river samples were collected and filtered almost immediately through a Nalgene filter unit with 0.45 μm cellulose nitrate membrane at Sites Q1 and Q2 (see Fig. 1) between DOY 328 (2003) and DOY 81 (2004). These dates encompass the entire runoff monitoring period, the earliest being taken after digging through to the base of the snowpack. In addition, when melting conditions were favourable, samples were also collected from moraines and talus deposits along the margin of the glacier (Sites T1, T2 and M1, M2, respectively).

Stable isotope sampling

For $^{15}N/^{14}N$, $^{34}S/^{32}S$ and $^{18}O/^{16}O$ analysis of NH_4^+, NO_3^-, and SO_4^{2-} 25 kg of snow or water were collected from four bulk snowpack samples (S1–S4, see above), a snow melt sample from above and within a basal slush zone at S1; eight proglacial river samples (four each at Sites Q1 and Q2) and single samples from Sites M1, M2, T1 and T2. Snowpack samples represented the complete section of snow down to the glacier surface, melted at 20°C. After 0.45 μm pressure filtering, samples were stripped of organics, cations and anions by passage through ISOLUTE Env$^+$ (International Sorbent Technology), and AG50W-X8 and AG2-X8 (Bio-Rad) resins (Heaton et al. 2004; Wynn et al. 2006, 7). Untreated samples were collected for $^2H/^1H$ and $^{18}O/^{16}O$ analysis of water.

DIC (dissolved inorganic carbon) for $^{13}C/^{12}C$ analysis was collected as barium carbonate by addition of alkaline barium chloride to samples of occasional runoff at the Sites Q1 and Q2, and spot samples at sites M1, M2, T1 and T2. The waters displayed no turbidity, and so they were not filtered prior to addition of barium chloride, avoiding possible loss of CO_2.

Hydrological monitoring

Hourly records of runoff (derived from a Druck pressure transducer), electrical conductivity and temperature measurements (Campbell 247 sensor) were collected at the proglacial river the Site Q1. At Site Q2, just electrical conductivity and water temperature records were collected. Pressure records were calibrated using the velocity area method and several different pressure-discharge rating curves with standard errors between 5 and 15% of mean discharge (see

Hodson 2006). We estimated from visual observations and three velocity-area discharge measurements that flow through the Site Q2 typically contributed 85% of the flow through Site Q1. A runoff time series at the Site Q2 was therefore constructed from 0.85 times the discharge at Site Q1.

Dissolution experiments

Dissolution experiments using freshly milled schist and phyllite-schist rock samples from the end moraine of Tuva Glacier were used to assess the broad characteristics of chemical weathering in high rock–water contact environments. Therefore, 10 g/L solutions were prepared after milling with a 250 μm sieve and added to 50 mL syringe tubes filled with deionised water and a 10 mL head space. The solutions were prepared in duplicate and agitated with an end-over shaker at 25°C for 24 h. Thereafter, they were centrifuged and the solutions decanted for immediate pH and ion analysis. New solutions were then prepared by resuspending the powders in deionised water and repeating the experiment twice. Alkalinity was estimated from charge balance for these experiments. Otherwise the analytical protocols employed were the same as those described below.

Analytical methods

Chemical analyses were either undertaken in Signy (NH_4^+ and NO_3^-) or the UK (all other tests) using protocols described in detail by Hodson (2006). Briefly, major cations were determined using either emission mode (Na^+, K^+) or absorption mode (Ca^{2+}, Mg^{2+}) atomic absorption spectroscopy following acidification with 2% HNO_3 and the addition of caesium chloride and lanthanum chloride for emission mode and absorption mode respectively. Dissolved silica was determined colourimetrically using the manual method molybdenum blue method reported by APHA (1995) and with a detection limit of 0.02 mg L^{-1}. The precision errors for all cation and Si determinations were ≤5%. Cl^- and SO_4^{2-} were quantified using a Dionex ICS2500 ion chromatograph after 2–4 months' dark, cool (4°C) storage. Precision errors were 7 and 6% at 40 μg L^{-1}, respectively. At Signy, and usually within 2 days of collection, we employed manual colorimetric tests for NH_4^+ (after Mackareth et al. 1978), and an automated Cd–Cu reduction, *N*-1-napthylethylenediamine procedure for NO_3^- (using a Skalar Autoanalyser). Detection limits were ca. 3 μgN L^{-1} for both determinations, whilst precision errors were ±10% for NH_4^+ and ±5% or less for NO_3^- (Hodson 2006). Tests of pH and HCO_3^- were also undertaken at Signy, making use of a Hach pH electrode calibrated with pH 4 and 7 buffer solutions and alkalinity titration, making use of 1 mM HCl and BDH mixed indicator (endpoint pH 4.5). Precision errors were 0.1 pH unit and 5% (HCO_3^-), respectively.

Stable isotope analysis

Resin columns were eluted using 1 M hydrobromic acid, with NH_4^+ processed to ammonium sulfate by the diffusion method, SO_4^{2-} recovered as barium sulfate, and NO_3^- processed to silver nitrate (Sigman et al. 1997; Chang et al. 1999; Hwang et al. 1999; Heaton et al. 2001, 2004; Wynn et al. 2005, 2006). $^{15}N/^{14}N$, $^{34}S/^{32}S$ and $^{18}O/^{16}O$ ratios, together with nitrate N/O atomic ratios, were determined by oxidative or reductive pyrolysis in elemental analysers coupled to a mass spectrometer (TC/EA-ConfloIII-Delta+XL system, ThermoFinnigan, Bremen, Germany). Values for $\delta^{15}N$ versus AIR, $\delta^{34}S$ versus CDT, and $\delta^{18}O$ versus SMOW were calculated by comparison with laboratory standards calibrated against international standards assuming: IAEA-N-1 $\delta^{15}N = +0.4‰$; NBS 127 $\delta^{34}S = +20.3‰$, $\delta^{18}O = +9.3‰$; IAEA-NO-3 $\delta^{18}O = +25.6‰$. The precision errors of laboratory standards (1 standard deviation) were ≤0.3‰ for $\delta^{15}N$ and $\delta^{34}S$, and ≤0.5‰ for $\delta^{18}O$.

$^2H/^1H$ ratios of water were determined by chromium reduction to hydrogen in a PyrOH elemental analyser (EuroVector, Milan) on-line to an Isoprime mass spectrometer (GV Instruments, Manchester, England), and $^{18}O/^{16}O$ ratios of water by equilibration with CO_2 in an Isoprep-18 online to a SIRA II mass spectrometer (VG Instruments, Middlewich, England). Values for δ^2H and $\delta^{18}O$ versus VSMOW were calculated by comparison with laboratory standards calibrated against VSMOW and SLAP. Precision of laboratory standards (1 SD) was ≤1‰ for δ^2H and ≤0.03‰ for $\delta^{18}O$.

Barium carbonate from DIC was reacted with phosphoric acid and the liberated CO_2 analysed in an

Optima dual-inlet mass spectrometer (VG Instruments, Middlewich, England). Values for $\delta^{13}C$ versus PDB were calculated by comparison with laboratory standards calibrated against NBS 19 and NBS 18 assuming NBS 18 $\delta^{13}C = -5.1‰$. Precision of laboratory standards (1 SD) was $\leq 0.1‰$.

Correction of $\delta^{18}O_{NO3}$ for organic matter

As in previous polar studies, contamination by dissolved organics caused problems for $\delta^{18}O_{NO3}$ analysis using the silver nitrate method (Heaton et al. 2004; Wynn et al. 2006, 2007; Tye and Heaton 2007). In this study the problem was particularly severe for the snowpit samples. We therefore estimated the $\delta^{18}O$ value of the contaminant by regression analysis of the measured $\delta^{18}O$ value of the contaminated silver nitrate against its N/O atomic ratio. The contaminant $\delta^{18}O$ value was identified by the origin of the *X* axis because analysis of the organics trapped on the Env^+ resin suggested that it contained no nitrogen. Since the $\delta^{18}O_{NO3}$ value for the uncontaminated end-member can be assumed to be similar for all the snowpits, and the N/O atomic ratio is 0.33 for pure nitrate, we were then able to correct each sample using its N/O atomic ratio (below). The regression model is shown in Fig. 2, and indicates a contaminant $\delta^{18}O$ value (i.e. N/O = 0) of +14.5‰, and a pure nitrate end-member (i.e. N/O = 0.33) of +49.5‰. This latter value is slightly lower than the range reported for nitrate aerosols at a coastal Antarctic station (Savarino et al. 2007).

$\delta^{18}O_{NO_3}$ values corrected for contamination were therefore calculated from the measured $\delta^{18}O$ values for silver nitrate, $\delta^{18}O_{measured}$, using:

$$\delta^{18}O_{NO_3} = \left(\delta^{18}O_{measured} - f_{organic} \times 14.5\right) / \left(1 - f_{organic}\right) \quad (1)$$

where the fraction of organic contaminant,

$$f_{organic} = 1 - \left[(N/O)_{measured}/0.33\right] \quad (2)$$

Corrected $\delta^{18}O_{NO3}$ values are presented together with $\delta^{18}O_{measured}$ values in the Results section. Thereafter, samples with high levels of contamination (N/O atomic ratios below 0.1), which are subject to large correction errors, are omitted from discussion and only corrected $\delta^{18}O_{NO3}$ values are considered for interpretation.

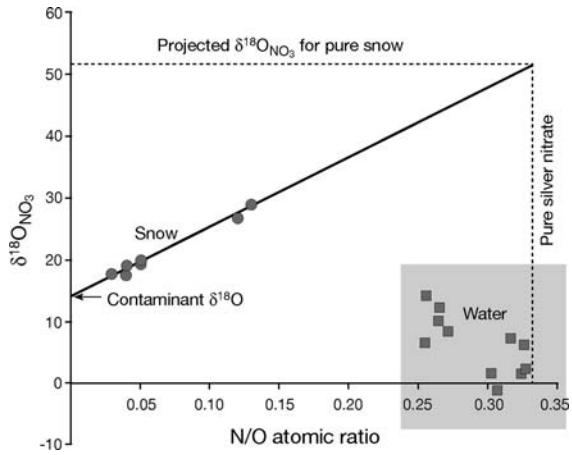

Fig. 2 N/O atomic ratios in silver nitrate recovered from the resin exchange columns and the corresponding $\delta^{18}O$. Ratios less than 0.33 show the presence of a contaminant rich in oxygen, yet lacking nitrogen. Thus the inferred $\delta^{18}O$ composition of the contaminant is assumed to lie where N/O = 0. The *shaded area* represents the domain occupied by water samples, collected from Sites Q1, Q2, T1, T2 and M2

Correction for marine salts

In order to establish the dynamics of rock weathering, estimates of non-snowpack solute concentrations were estimated for each sample. The concentrations of all cations, SO_4^{2-}, NH_4^+ and NO_3^- derived from non-snowpack sources were therefore defined thus:

$$^*X = X - a\mathrm{Cl}^- \quad (3)$$

where $^*X$ is the non-snowpack concentration of solute *X* and *a* is the ratio of solute *X* to Cl^- in bulk snowpack and snowmelt (from a lysimeter at Site S1) in Tuva Glacier basin, as reported by Hodson (2006). However, for NO_3^- and NH_4^+ only pre-melt bulk snowpack data were used to define *a* (the values being 0.0051 and 0.0072 with equivalent units) on account of the fact that microbial assimilation of these ions affected the ratios in the snowmelt (Hodson 2006). Inclusion of the snowmelt samples in the estimation procedure (for ions other than NO_3^- and NH_4^+) was important because it allowed us to use data that spanned a far greater range of concentrations than that afforded by just the bulk snow samples. Such a range was necessary due to the strong elution process that occurred during snowmelt, which caused early runoff to be markedly more concentrated than the snowpack (see Hodson 2006). Interestingly, the preferential elution of certain

solutes over Cl^- was found to be negligible according to this work, giving much confidence in our ability to remove the large snowpack-derived contribution of the solutes using these Cl^- ratios.

The liberation of solute from non-snowpack sources was further characterised by estimating fluxes of $*X$ (in g d^{-1}) from the product of daily runoff volume and non-snowpack solute concentration. Where necessary, linear interpolation was used to fill in any gaps in the daily concentration series (see Hodson 2006). The annual fluxes (F_{tot}) of $*X$ were then estimated using:

$$F_{tot} = \sum_{i=1}^{i=n} (Q_{dtot}{}^{*}X_i) \quad (4)$$

where F_{tot} = total solute flux (g); Q_{dtot} = total discharge for individual days (m^3 day^{-1}); $*X_i$ = non-snowpack concentration of single daily sample (mg L^{-1}). n = number of days in observation period.

The fluxes (g a^{-1}) of $*Ca^{2+}$, $*Mg^{2+}$, $*Na^+$, $*K^+$ $*NH_4{}^+$, $*NO_3{}^-$ and $*SO_4{}^{2-}$ were then transformed into mass yields (kg km^{-2} a^{-1}) and cation yields ($\Sigma *M^+$ m^{-2} a^{-1}) in order to compare the results of this work with other studies, including the more detailed mass balance results presented by Hodson (2006) for Tuva Glacier. Since neither Si nor $HCO_3{}^-$ were detected in the snowpack, their total runoff yields were estimated instead.

Results

Non-snowpack solute transfer

Figure 3 shows the discharge and daily concentrations of total snowpack and non-snowpack cation concentrations ($^{snow}M^+$ and $*M^+$, respectively). A distinct seasonal hydrograph is evident, with an early season low flow phase (prior to DOY 6, 2004), a mid-season high flow phase thereafter (until DOY 28, 2004) and a final low-moderate flow phase until DOY 82, 2004. Both sources of cations declined throughout these stages of the runoff season. However, the relative importance of $*M^+$ grew due to a more rapid decline in $^{snow}M^+$. Figure 4 presents the cumulative fluxes of $^{snow}M^+$ and $*M^+$. The first 50% of $^{snow}M^+$ was transported by the first 25% of runoff and thus typical of a strong snowpack elution process (see Hodson 2006). By contrast, the first 50% of $*M^+$ required 70% of the total annual runoff. However, concentrations of $*M^+$ were still significant in the early low flow phase, as were dissolved Si concentrations (Fig. 3), which showed high values in the very first samples (up to 9 μM). Therefore rock–water interactions were an important source of solute to runoff throughout the entire summer. Overall, they contributed 42% of total cation transfer, the rest being accounted for by $^{snow}M^+$.

Table 1 shows the yields of non-snowpack ions, Si and $HCO_3{}^-$. The non-snowpack yields are also compared to estimates produced by Hodson (2006), who used summer bulk deposition estimates and changes in snow pack water equivalent and chemistry (rather than ratios to Cl^-) to remove atmospheric solute inputs. Solute mass export from non-snowpack solute sources appears to be dominated by $HCO_3{}^-$, $*Na^+$ and then $*Ca^{2+}$. When all concentrations are combined, chemical denudation estimates of 5.2 and 6.8 tons km^{-2} a^{-1} are evident for the Q2 and Q1 catchments respectively, if rock weathering is assumed to account for all non-snowpack solute delivery except $*NO_3{}^-$ and $*NH_4{}^+$. No attempt here has been made to assess the $HCO_3{}^-$ derived from organic and atmospheric sources and so more appropriate measures for assessing the efficacy of chemical denudation might be the equivalent cation yields, which were 160 and 130 meq m^{-2} a^{-1} for Sites Q1 and Q2. The ratio Q2/Q1 for the $*X$ yields is also shown in Table 1 as a proxy for solute sources and sinks in the glacier forefield. Values <1 reveal that the glacial forefield, which showed little evidence of recent glaciation, plays an important role in moderating $*X$ transfer to the coast. Thus $*NH_4{}^+$ sequestration, $*NO_3{}^-$ production and chemical denudation (all cations and $*SO_4{}^{2-}$) are distinct features of these ratios, whilst $HCO_3{}^-$ yields appear unchanged.

Cation composition

When expressed in equivalent units, seasonal changes in the cation composition of runoff at the Site Q1 reveal variable concentrations of $*K^+$ and $*Na^+$, which are greatest in the latter stages of the ablation season. In contrast, $*Ca^{2+}$ and $*Mg^{2+}$ concentrations are more stable and appear to decrease during the first half of the ablation season (until DOY 28, 2004) and rise again afterwards. This results in $*Ca^{2+}$ being the

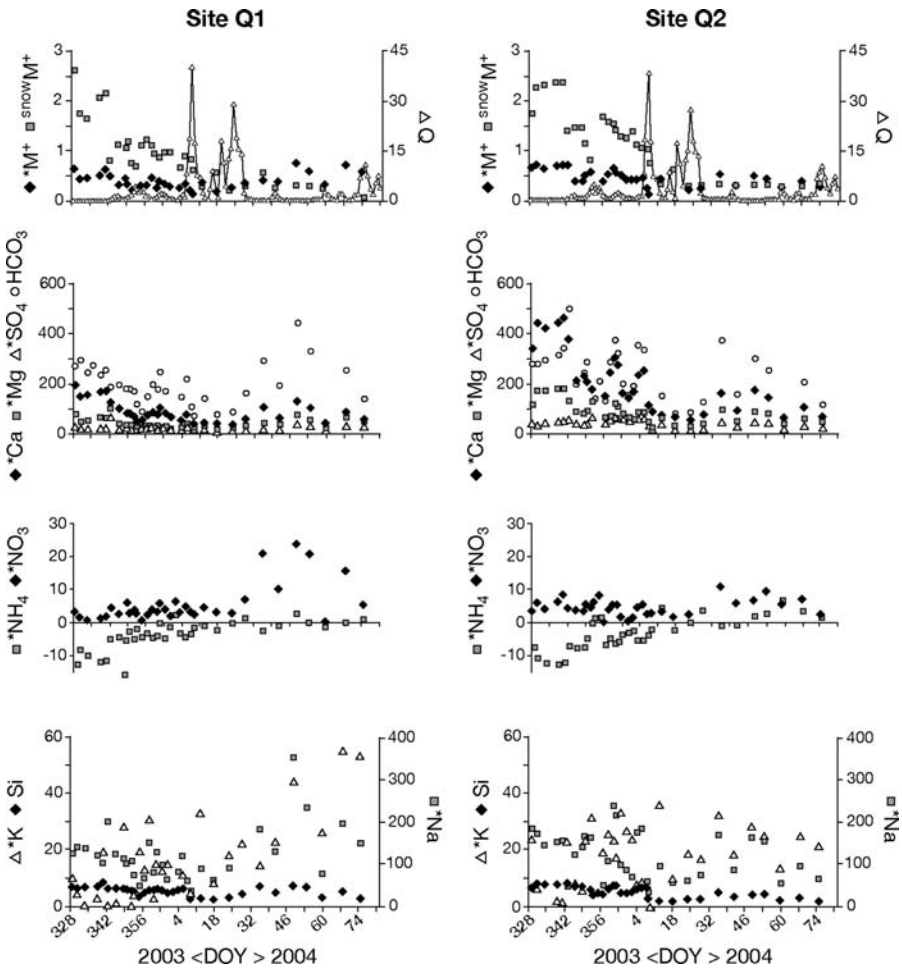

Fig. 3 Daily runoff (Q, in $m^3 \times 10^3$ day^{-1}), the sum of snowpack ($^{snow}M^+$) and non-snowpack ($*M^+$) cation concentrations and the concentrations of all major, dissolved constituents corrected for snowpack inputs (not necessary for HCO_3^- and Si). Units of concentration are meq L^{-1} ($^{snow}M^+$ and $*M^+$), μeq L^{-1} and μM (Si only)

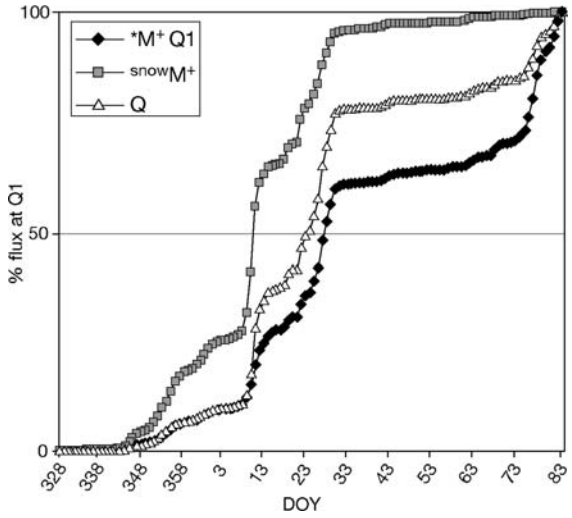

Fig. 4 Cumulative runoff and solute fluxes at Q1 expressed as a percentage of the total (see Table 1 for actual yields)

dominant ion in the early low flow period, and $*Na^+$ dominating the remainder of the observation period. A similar pattern can be inferred from the Site Q2 cation series, although the decrease in $*Ca^{2+}$ is more pronounced. The variable $*Na^+$ and $*K^+$ concentrations early in the observation period may be erroneous on account of this being the stage of the ablation season when marine sources were of greatest importance. Any errors in the marine salt correction would therefore have greatest impact here. However, if this error was large, the $*Na^+$ and $*K^+$ yields would most likely differ markedly between the present study and those reported by Hodson (2006) (see Table 1). The differences in Table 1 suggest that a small $*K^+$ flux has been underestimated by the present study, whilst the greater $*Na^+$ flux is consistent with the estimate of Hodson (2006) and therefore implies that Na^+ liberation by dissolution is a major process occurring

Table 1 Solute yields from non-snowpack sources, including mass yields and total equivalent yields for the cations (Σ*meq^{+} km^{-2} a^{-1})

Solute	Q2 This study (kg km^{-2} a^{-1})	Q1 This study (kg km^{-2} a^{-1})	Q1 Hodson (2006) (kg km^{-2} a^{-1})	Q2/Q1 yield ratio
Si	38.3	44.0	47.2	0.87
*Mg	196	254	191	0.77
*Ca	739	833	865	0.89
*Na	1,185	1,389	1,490	0.85
*K	156	209	253	0.75
*SO_4	493	579	590	0.85
HCO_3	3,067	3,060	–	1.00
Sum of above	5,166	6,750		0.77
*NH_4	−4.5	−12	−25	0.38
*NO_3	21	34	30	0.62
Σ*meq^{+} km^{-2} a^{-1}	129	163	131	0.79

Negative values represent solute sinks within the catchment

in the Tuva Glacier basin. Lastly, concentrations of *Na^{+}, *Ca^{2+} and *Mg^{2+} were highest at Site Q1 towards the end of the observation period, so we also suggest that the cation dissolution in the glacier forefield had a more marked effect after the removal of its seasonal snow and icing cover.

Major anion composition and CO_2 partial pressures

Variations in the molar ratio *SO_4^{2-}/HCO_3^{-} at both Sites Q2 and Q1 reveal a change in the anion composition of runoff (Fig. 5a). The *SO_4^{2-}/HCO_3^{-} ratio was low at the start of the runoff period, but generally increased until the onset of the high flow phase (DOY 6, 2004), when values dropped again. Thereafter the *SO_4^{2-}/HCO_3^{-} ratio began to recover during the late low flow phase around DOY 36 (2004), especially at Site Q1. Figure 5b also presents the partial pressure of CO_2 (hereafter expressed as $\log_{10}$ p(CO_2)) which was estimated using PHREEQC speciation modelling (Parkhurst 1995). The $\log_{10}$ p(CO_2) values decreased throughout the first half of the observation period, especially following the onset of high flows on DOY 341 (2003), reaching values that were close to atmospheric equilibrium (i.e. ca. $10^{-3.5}$ atmospheres) around DOY 10 (2004). The high $\log_{10}$ p(CO_2) and low *SO_4^{2-}/HCO_3^{-} ratio at both sites during the early season low flow phase therefore identify an additional source of HCO_3^{-} to runoff early in the summer that diminishes in importance as runoff increases. Later on in the summer, the increase in both $\log_{10}$ p(CO_2) and *SO_4^{2-}/HCO_3^{-} appears more significant at Site Q1, suggesting that processes in the forefield were influencing both these terms.

Nitrogen biogeochemistry

Figure 3 shows time series of *NH_4^{+} and *NO_3^{-}. The dynamics of these nutrients are broadly similar at the Sites Q1 and Q2, showing a deficit (−ve values) of *NH_4^{+} during the early low flow phase, when *NO_3^{-} concentrations were positive and quasi-stable. The high flow phase in the middle of the observation period was characterised by lower *NO_3^{-} concentrations at Site Q2, whilst high values returned afterwards, reaching seasonal maximum values at Site Q1. However, *NH_4^{+} concentrations, despite increasing progressively through the entire observation period, were low and only reached values significantly above zero at Site Q2 after the high flow phase.

Chemistry and stable isotopes of C,N,O and S

Tables 2 and 3 present the chemical and stable isotope data for snow, snowpack water, runoff and spot water samples collected from the talus water and moraine water. Averages of these data are also shown for bulk snow, runoff at Sites Q2 and Q1 and combined talus/moraine water in Fig. 6. Snow samples show low $\delta^{15}N$ values for both NH_4^{+} and NO_3^{-} (although the latter also shows considerable variability), whilst Q1 shows higher $\delta^{15}N$, especially in the case of NH_4^{+}. However, differences in the stable isotope values for ^{15}N are minor, especially when compared to the

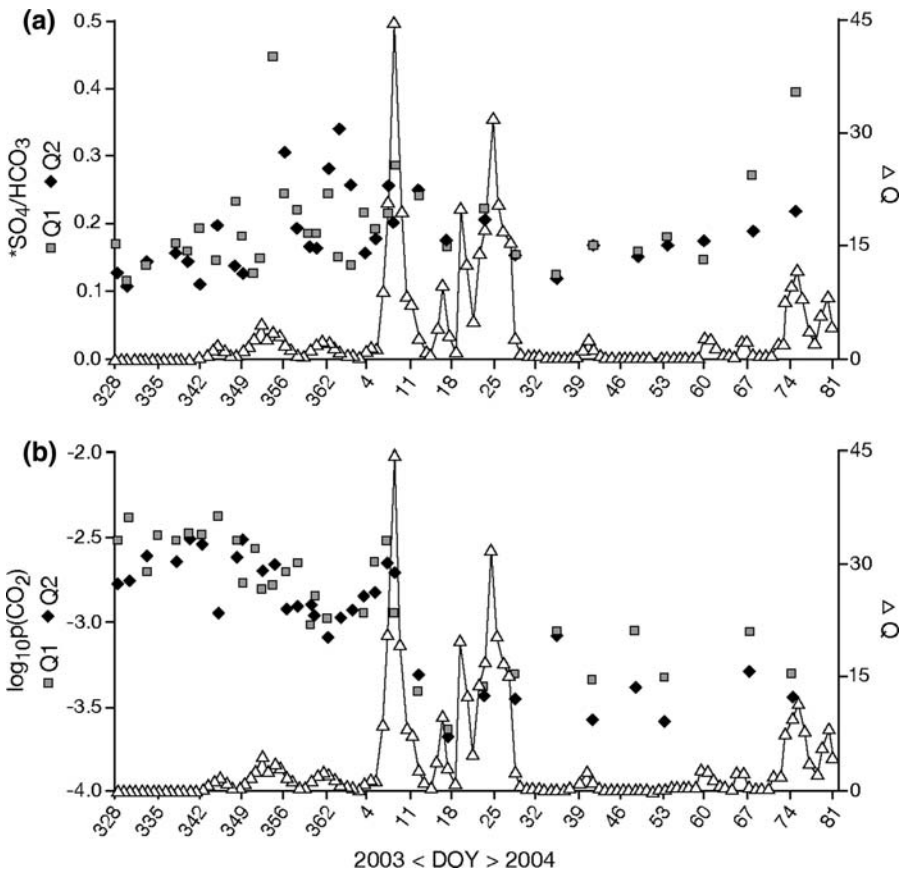

Fig. 5 Discharge and **a** molar ratios of $*SO_4^{2-}$ to HCO_3, **b** $\log_{10}$ $p(CO_2)$ at Sites Q1 and Q2

$\delta^{18}O_{NO_3}$ values. Here, the corrected $\delta^{18}O_{NO_3}$ of snow and snowmelt (Table 3) are far greater than values from M2, T1 and T2. Values from Q1 and Q2 are also low and are only just greater that the M2, T1 and T2 samples. The talus/moraine waters also produce the lowest $\delta^{34}S$ ($+9.5 \pm 2.8‰$) and $\delta^{18}O_{SO_4}$ ($+1.2 \pm 1.2‰$), which are significantly different from the snow data (average $\delta^{34}S = 19.3 \pm 0.28‰$; average $\delta^{18}O_{SO_4} = +8.5 \pm 0.19‰$). Low standard deviations for Snow $\delta^{34}S$ and $\delta^{18}O_{SO4}$ (Fig. 6) also indicate that SO_4^{2-} isotopes displayed the least spatial variation across the catchment snowpack. Values of $\delta^{13}C$ could not be defined for the snowpack due to low DIC. However, there are clear differences in the $\delta^{13}C$ of other sample types, with higher values in the talus/moraine water. Lastly, $\delta^{18}O$ values (for water) indicate that snowpack waters are generally highest (average $-11.0‰ \pm 0.84$), whilst all other water types are typically only 1‰ lower. Thus there is no evidence of significant evaporative enrichment of waters in the high rock–water contact zones of the catchment, as is observed in parts of continental Antarctica (Gooseff et al. 2002).

Discussion

Seasonal melting, flowpaths and the concentrations of non-snowpack ions

The data presented above describe a catchment that maintained a high degree of snow cover throughout the runoff season. A modest quantity of runoff was observed (ca. 0.53 m a^{-1} according to Hodson (2006)), the vast majority of which was snowmelt, rather than ice melt and rainfall. The seasonal hydrograph presented in Fig. 3 clearly shows the dominance of the high flow phase between DOYs 7 and 28, 2004, when $p(CO_2)$ values moved closer to atmospheric equilibrium and $*SO_4^{2-}/HCO_3^-$ ratios declined (Fig. 5). These peak flows were supplied by the meltwaters impounded for some time within a

Table 2 Solute concentrations in samples that were collected from snowpit sites (S1–S4), talus water (T), moraine water (M) and bulk runoff (Q1 and Q2) and subject to isotopic analysis

Description	pH	Cl (μeq/L)	HCO_3 (μeq/L)	Si (μM)	Ca Total/non-snowpack (μeq/L)	SO_4^{2-}	NO_3^-	NH_4^+
S1 DOY 328	5.87	88	–	0	3.5/–	11/–	0.32/–	0.23/–
S2 DOY 317	5.85	42	–	0	1.0/–	4.5/–	0.17/–	0.26/–
S3 DOY 320	6.12	160	–	0	4.8/–	18/–	0.35/–	0.55/–
S4 DOY 328	5.87	71	–	0	1.8/–	7.1/–	0.49/–	0.61/–
S1 melt DOY 365	6.21	900	–	0	390/–	1,150/–	10/–	10/–
S1 slush DOY 351	5.91	8,700	–	0	42/–	130/–	3.5/–	16/–
Q1 DOY 340	6.66	2,000	180	8.3	400/330	270/40	11/1.4	0.53/−11.7
Q1 DOY 349	6.79	1,100	170	6.0	200/160	160/31	7.7/2.6	4.0/−2.8
Q1 DOY 358	6.72	1,000	190	5.9	200/170	160/42	8.5/3.7	1.9/−4.5
Q1 DOY 2 (2004)	6.73	920	140	5.1	190/120	143/35	6.0/6.0	2.3/2.3
Q2 DOY 340	6.73	2,100	490	9.7	530/460	120/48	18/8.1	0.34/−12
Q2 DOY 349	6.66	950	280	6.6	240/200	150/35	9.7/5.2	1.1/−4.7
Q2 DOY 358	7.05	1,354	278	6.51	290/240	210/54	9.8/3.5	3.2/−5.1
Q2 DOY 2 (2004)	6.89	1,191	346	5.33	210/160	180/47	6.3/0.81	4.7/−2.6
Q4 DOY 4 (2004)	7.33	200	397	6.64	310/300	68/45	6.4/6.4	0.14/−1.1
T1 DOY 363	7.44	1,275	782	11.87	880/820	291/140	15/8.5	2.1/−5.7
T2 DOY 363	7.54	776	733	14.36	533/500	160/69	12/9.4	0.0/−4.7
M1 DOY 4 (2004)	6.34	670	181	5.6	150/120	109/30	6.4/3.7	1.1/−3.0
M2 DOY 6 (2004)	7.14	202	510	5.61	180/170	69/45	6.7/6.1	0.39/−0.84

Dates are given as day numbers (DOY) for 2003 unless otherwise indicated

small lake at the ice/end moraine margin and described by Hodson (2006). The storage of these waters most likely enabled equilibration with atmospheric CO_2 conditions in a low rock–water contact environment, because these conditions prevailed at Sites Q2 and Q1 when these lake waters outburst into the stream. However, far more interesting geochemical conditions appear to exist before this lake outburst, including high concentrations of non-snowpack ions, $p(CO_2)$ values in excess of atmospheric equilibrium and increasing $*SO_4^{2-}/HCO_3^-$ ratios during the early low flow phase. These are strongly diagnostic of solute acquisition along flowpaths that afford extended rock–water contact, producing seasonal maximum levels of dissolved Si on DOY 361, 2003 at Site Q2 in spite of levels of Si being below detection in even the most concentrated snowmelt sampled upon the glacier. Respiration of organic carbon along such flowpaths might also explain the high $p(CO_2)$ conditions in this early runoff phase, although the $\delta^{13}C_{DIC}$ values do not support this (see below). Thus delayed flowpaths that afford intimate rock–water contact dominated runoff before the lake outburst. Direct field observations showed that these were mostly due to snowmelt infiltration into moraines and talus deposits along glacier margins (Fig. 1). Further, the removal of the snowcover and icings from the intervening forefield and proglacial water course between Sites Q2 and Q1 also coincided with noticeable inputs of rock weathering ions during the late low flow phase (after DOY 28, 2004). The concentration of many solutes therefore increased downstream during this interval. In summary, our data show that solute acquisition was initially most important in the talus and moraine covered parts of the upper catchment and of increasing importance in the downstream forefield thereafter.

Carbonate weathering and its coupling to pyrite oxidation

Carbonate weathering is a major solute source to runoff at retreating glacier margins (Wadham et al. 2001; Cooper et al. 2002; Anderson et al. 2000) which should, therefore, be considered in the context of the present study. Potential sources of carbonate

Table 3 Stable isotope data for the samples in Table 2

Description	$\delta^{15}N$–NH_4 vs. air	$\delta^{15}N_{NO_3}$ vs. AIR	$\delta^{18}O_{NO_3}$ vs. SMOW	N/O ratio	Corrected $\delta^{18}O_{NO_3}$	$f^*NO_3^-$	$\delta^{34}S_{SO_4}$ vs. CDT	$\delta^{18}O_{SO_4}$ vs. SMOW	$\delta\ ^{13}C_{DIC}$ vs. PDB	$\delta^{18}O$ vs. SMOW	δD vs. SMOW	$*\delta^{18}O_{SO_4}$	$f^*SO_4^{2-}$
S1 DOY 328	+3.5	−1.58	+18.2	0.03	(60.32)	0	+19.6	+8.3	n.d.	−10.10	−73.9	–	0
S2 DOY 317	+5.9	−2.04	+28.9	0.13	52.64	0	+19.3	+8.7	n.d.	−10.58	−79.9	–	0
S3 DOY 320	+7.9	+2.13	+18.4	0.04	(49.39)	0	+19.1	+8.5	n.d.	−11.16	−83.0	–	0
S4 DOY 328	+4.0	−4.60	+19.0	0.04	(51.31)	0	+19.1	+8.6	n.d.	−12.05	−90.4	–	0
S1 melt DOY 365	−2.3	−7.62	+26.7	0.12	48.48	0	+19.9	+9.5	n.d.	−14.17	−107.5	–	0
S1 slush DOY 351	+9.1	−5.49	+19.5	0.05	(51.66)	0	+20.0	+8.8	n.d.	−13.21	−96.9	–	0
Q1 DOY 340	+8.5	−1.47	+5.8	0.32	5.60	0.13	+17.5	+6.1	−5.0	−11.36	−84.6	−9.6	0.15
Q1 DOY 349	+10.9	−0.13	+9.7	0.26	8.52	0.33	+17.1	+5.3	n.d.			−9.4	0.20
Q1 DOY 358	+6.4	+0.11	+6.7	0.31	6.19	0.43	+17.2	+6.2	−2.9	−11.63	−87.5	−1.4	0.26
Q1 DOY 2 (2004)	+7.7	−1.37	+11.5	0.26	10.85	0.00	+17.6	+6.3	n.d.	−12.52	−94.5	−0.5	0.27
Q2 DOY 340	+10.2	−0.83	+1.5	0.32	1.12	0.46	+17.1	+5.6	−3.4	−11.34	−83.8	−10.9	0.17
Q2 DOY 349	+6.5	−1.15	+6.0	0.25	3.46	0.54	+16.0	+5.7	−3.9	−10.74	−79.9	−4.0	0.24
Q2 DOY 358	+3.3	−1.30	+8.1	0.27	6.67	0.36	+16.5	+5.6	−3.7	−11.82	−88.6	−4.1	0.26
Q2 DOY 2 (2004)	+6.9	−2.11	+13.6	0.25	13.59	0.13	+17.8	+6.6	−2.6	−12.81	−95.5	−0.1	0.25
T1 DOY 363						0.55			−3.1				
T2 DOY 363	+4.6	+0.44	+0.9	0.30	−0.55	0.70	+8.7	+0.8	−0.0	−11.89	−90.4	−7.9	0.48
M1 DOY 4 (2004)	+2.8	−1.31	−0.8	0.31	−2.10	0.85	+12.6	+2.4	−1.4	−10.93	−83.9	−6.1	0.43
M2 DOY 6 (2004)	–	–	–	–	–	0.06	–	–	−1.8	–	–	–	0.65
T1 DOY 363	+6.6	−1.50	+1.1	0.32	0.61	0.13	+7.3	+0.2	−2.9	−12.92	−100.4	−4.4	0.65

"Corrected $\delta^{18}O_{NO_3}$" denotes corrected values following Eqs. 1, 2. Samples deemed too contaminated (N/O < 0.1) are in parenthesis. See text for explanation. "n.d." denotes "not detected" due to insufficient capture of $BaCO_3$. Values of $*\delta^{18}O_{SO_4}$ that are underlined indicate sub-oxic production of $*SO_4^{2-}$ (see text for explanation). $f^*NO_3^-$ is the ratio $*NO_3^-$/total NO_3^- and $f^*SO_4^{2-}$ is the ratio $*SO_4^{2-}$/total SO_4^{2-}

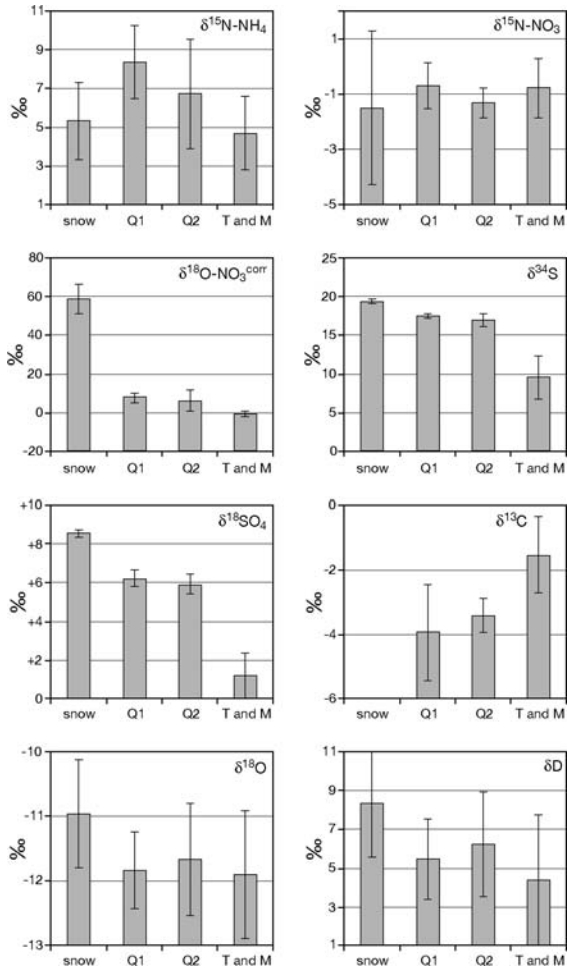

Fig. 6 Average and standard deviation (*error bars*) of the stable isotope data for snow, runoff at Q1 and Q2 and the lumped talus (T) and moraine (M) waters

for weathering in the Tuva Glacier basin include marbles that are dispersed as minor outcrops among the schists (Mathews and Maling 1967). They have, however, been overlooked by Hall et al. (1986), who conducted a dissolution experiment with Signy Island schist powders and attributed the release of Ca^{2+} to plagioclase instead. In his study, the dissolution of Ca^{2+}-deficient rock powders from a different part of the island was studied, producing solutions that were dominated by $*Na^{+}$ and also attributed to plagioclase. However, our own closed-system dissolution experiments, conducted in a with two different schist-derived rock powders from the Tuva Glacier end moraine, produced clear evidence of carbonate dissolution (see Table 4) and calcite saturation according to PHREEQC speciation modelling (data not shown). The high rock–water contact ratios of the dissolution experiments (10 g L^{-1}) almost certainly contributed to the saturation of calcite weathering products though, and it should be noted that PHREEQC modelling indicated no saturation with respect to calcite in water samples collected during field work. However, high $*Ca^{2+}$ concentrations clearly suggest that carbonate dissolution is a significant early season reaction in the present study, producing the second greatest cation yield (833 kg km^{-2} a^{-1} at Site Q1) after *Na (1,400 kg km^{-2} a^{-1}: see Table 1). Stable isotope data also reveal isotopically heavy $\delta^{13}C_{DIC}$ values in moraine and talus waters that are strongly diagnostic of carbonate weathering, because they are close to 0‰ and the other samples from sites with less evidence of rock contact (i.e. Q1 and Q2) are isotopically lighter than the VPDB carbonate standard (Fig. 6; Table 3).

Equation 5 and Fig. 5a suggest that the coupling of carbonate dissolution and sulphide oxidation is likely to be weak in the Tuva Glacier system, because low $*SO_4^{2-}/HCO_3^{-}$ molar ratios existed. According to Eq. 5, ratios of 0.5 are to be expected when carbonate dissolution in dilute waters neutralises all protons liberated by sulphide oxidation. Limited exposure or abundance of reactive sulphide mineral surfaces might be responsible, as well as slow rates of production by mechanical comminution (perhaps reflecting the lack of rock–water contact at the glacier bed). Studies from the cold-based Austre Brøggerbreen glacier in Svalbard yielded similar, low $*SO_4^{2-}/HCO_3^{-}$ ratios, despite the presence of sulphide minerals in the local rocks (Hodson et al. 2002). Elsewhere in glacial environments where temperate glaciers offer intimate contact along subglacial flowpaths, the $*SO_4^{2-}/HCO_3^{-}$ is much greater, approaching 0.5 in some cases (i.e. the stoichiometry of Eq. 5; Tranter et al. 1996). The dissolution results in Table 4 suggest that $*SO_4^{2-}$ liberation produces low $*SO_4^{2-}/HCO_3^{-}$ ratios (0.03 or less) even when the rock–water contact ratio is high (10 mg L^{-1}). This suggests that low S abundance in rocks is sufficient to explain the low $*SO_4^{2-}/HCO_3^{-}$ ratios in Tuva Glacier runoff. A beta probe analysis of two Signy Island powders using scanning electron microscopy and described in Hall et al. (1986) also supports this assertion, since levels of S were below detection in one sample and just 4% in another. However, a lack of information on the

Table 4 Chemistry of solutions produced by closed system dissolution experiments using Tuva Glacier moraine rock flour: "a" and "b" denote duplicate pairs from separate experiments repeated three times (1st, 2nd, 3rd)

(μeq L^{-1})	Cycle	pH a	pH b	Ca a	Ca b	Mg a	Mg b	Na a	Na b	K a	K b	SO_4 a	SO_4 b	Alk a	Alk b
Mica-Schist	1st	8.47	8.47	273	282	13.8	14.1	41.2	47.5	87.2	94.4	12.01	13.62	401	422
	2nd	9.28	9.53	276	279	10.5	10.7	7.8	6.2	78.7	81.0	1.26	1.28	371	375
	3rd	9.1	9.26	150	207	8.1	12.0	2.3	3.1	51.3	57.4	0.98	0.95	210	278
Phyllite-Schist	1st	8.56	8.96	322	357	22.8	22.0	29.6	33.8	11.2	10.1	1.98	2.98	381	417
	2nd	9.59	9.47	326	324	18.1	20.6	4.3	5.7	4.8	5.6	0.32	0.60	353	354
	3rd	9.6	9.53	345	347	14.8	16.4	2.5	2.6	3.4	3.8	0.26	0.23	364	369

"Alk" means alkalinity estimated by charge balance. The experimental process included milling and removal of >250 μm particles, followed by closed system dissolution at 40 g/L concentration in a 50 mL vial (with a 10 mL head space) for 1 day using an end-over shaker at 25°C

source of samples used for this analysis make it difficult to place these data in the context of the present study.

$$4FeS_{2(s)} + 16CaCO_{3(s)} + 15O_{2(aq)} + 14H_2O_{(l)} = 16Ca^{2+}_{(aq)} + 16HCO^{-}_{3(aq)} + 8SO^{2-}_{4(aq)} + 4Fe(OH)_{3(s)} \quad (5)$$

Re-wetting of the rock powders during our dissolution experiments demonstrated a marked decrease in the liberation of SO_4^{2-} from the two different schist samples that were considered (Table 4). This might indicate that dissolution of a non-renewable source of $*SO_4^{2-}$ such as marine salts or even secondary anhydrite was responsible for $*SO_4^{2-}$ liberation, rather than sulphide oxidation. The formation of surficial secondary salts following evaporitic concentration is well known in arid polar catchments (e.g. Cooper et al. 2002; Meiklejohn and Hall 1997) and should not be precluded in the present study due to the high rates of marine salt deposition on the catchment (Hodson 2006). Therefore, further confirmation of the process of sulphide oxidation was sought using the stable isotopes. These data (Table 3) show high $\delta^{34}S_{SO_4}$ relative to the snowpack in talus and moraine waters, suggesting that the primary source of the S was indeed crustal, rather than marine. If marine sources of sulphate are assumed to have $\delta^{34}S$ values of ca. +19 to +20‰, as suggested by the snowpack values (which are close to the average value of +21‰ for ocean water SO_4^{2-}; Rees et al. 1978), then marine sulphate appears dominant in the proglacial stream waters (Q1 and Q2) which have similarly high $\delta^{34}S$ values. In contrast, a greater proportion of $*SO_4^{2-}$ is indicated for the talus/moraine waters due to their higher SO_4^{2-}/Cl^- ratios, and significantly lower $\delta^{34}S$ values. Simple mass balance calculations according to Eq. 3 suggested that the proportion of $*SO_4^{2-}$ lay between 60 and 80% of the total for these isotopically distinct samples (Table 3). Since no sources of $*SO_4^{2-}$ other than pyrite exist are known within the host rocks, we suggest all the $*SO_4^{2-}$ in our runoff samples and dissolution experiments may be attributed to the oxidation of sulphides. The process is most likely limited by low abundance in these rocks and might also be limited by slow reactive surface area regeneration (Brown et al. 1996).

Fe and $*SO_4^{2-}$ liberation: fingerprints of microbial weathering?

The presence of low yet detectable levels of $*SO_4^{2-}$ from a probable sulphide source is significant for two key reasons. First it necessitates consideration of the potential for weathering to liberate Fe to runoff, and second it presents a basis for exploring whether microbial activity plays a role in rock weathering reactions in Tuva Glacier basin during the melt season. Continental Fe fertilisation of the Southern Ocean ecosystem is an important issue (e.g. Raiswell et al. 2006; Watson et al. 2000) and so levels of dissolved Fe were determined opportunistically for a limited number of samples using ICP MS (samples were acidified and the detection limit was 1 μg L^{-1}: see Table 5). These data clearly show levels of dissolved Fe close to detection in snow but ca. 17 μg L^{-1} in the moraine and talus waters. Dissolved Fe mobilisation therefore takes place in high rock–water contact environments, but, according to Table 5, only produces low concentrations in bulk runoff (ca. 3 μg L^{-1}). Data on the Fe

Table 5 Total dissolved Fe (μg/L) according to ICP-MS

	Bulk snow	Bulk deposition	Talus and Moraine	Site Q1
Mean	0.99	1.30	17.40	3.43
SD	1.66	1.53	0.30	4.31
n	37	7	7	15

"SD" denotes the standard deviation and "*n*" is the number of samples analysed. All samples collected prior to DOY 8, 2004

content of glacial runoff are sparse, having received detailed research attention in the first instance from Mitchell et al. (2001) in a study of Alpine glacial meltwaters (15–1,200 μg L^{-1}, median 380 μg L^{-1}). Yde and Knudsen (2004) and Yde et al. (2005, in press) described dissolved Fe concentrations in three Greenland glacial catchments (30–1,800 μg L^{-1}), whilst more recently, Statham et al. (2008) have assessed the Fe content of dilute runoff from part of the Greenland Ice Sheet. The latter found total dissolved Fe concentrations much lower than those reported by Yde and Knudsen (2004) and Yde et al. (2005) at ~2.96 μg L^{-1}, and thus almost identical to the present study. These studies coupled with the above experimental evidence therefore suggest that relatively low dissolved Fe concentrations in bulk runoff from Tuva Glacier are due to a combination of dilution by glacial meltwater and a lack of reactive pyrite and other Fe-bearing minerals along runoff flowpaths. However, the solubility of Fe in pH-neutral, oxygenated environments is also very low and so the higher concentrations in talus and moraine waters might indicate Fe liberation in anoxic weathering environments. We therefore used $\delta^{18}O_{SO_4}$ to consider whether such conditions exist, following the rationale of Bottrell and Tranter (2002). This defines a threshold value for $\delta^{18}O_{SO_4}$, $\delta^{18}O_{threshold}$, below which $\delta^{18}O_{SO_4}$ values suggest production of $*SO_4^{2-}$ in sub-oxic conditions:

$$\delta^{18}O_{threshold} = \left[\left(\delta^{18}O_{atmosO_2} - 8.7\right) \times 0.25\right] + \left(0.75 \times \delta^{18}O_{H_2O}\right) \quad (6)$$

where $\delta^{18}O_{atmosO2}$ is the $\delta^{18}O$ of atmospheric O_2 (+23.5‰ after Kroopnick and Craig 1972) and $\delta^{18}O_{H_2O}$ is the $\delta^{18}O$ of water, defined by our own analyses. The calculation assumes that water is the only source of oxygen for sulphide oxidation under anoxic conditions, whilst both water and air O_2 are available if oxic conditions prevail. An isotopic enrichment of −8.7‰ during the incorporation of O_2 from the atmosphere and into $*SO_4^{2-}$ was also assumed. In the present study, for $\delta^{18}O_{H_2O} = -11$ to −13‰ (Table 3), $\delta^{18}O_{threshold}$ values were −4.3 to −5.9‰ and so only the talus $\delta^{18}O_{SO_4}$ raw values lay close to this threshold (Table 3). However, even in these samples, appreciable concentrations of Cl^- (see Table 3) indicate the presence of snowpack SO_4^{2-}, necessitating the correction:

$$*\delta^{18}O_{SO_4} = \left[\delta^{18}O_{SO_4} - \left(\delta^{18}O_{SO_4}^{snow} \times f_{SO_4}^{snow}\right)\right] / \times \left(1 - f_{SO_4}^{snow}\right)$$

where $*\delta^{18}O_{SO_4}$ is the calculated value for $*SO_4^{2-}$ (ie SO_4^{2-} produced by weathering), $\delta^{18}O_{SO_4}$ and $\delta^{18}O_{SO_4}^{snow}$ are the measured values in the water and in snow, and $f_{SO_4}^{snow}$ is the fraction of snowpack-derived SO_4^{2-} calculated using Eq. 3. The values of $*\delta^{18}O_{SO_4}$ are given in Table 3 and they are below $\delta^{18}O_{threshold}$ in the earliest samples of runoff from Q1, Q2 and also in talus water (T1). Sub-oxic, microbially mediated production of $*SO_4^{2-}$ is therefore a distinct feature of rock–water contact early in the runoff season. Presumably, the weathering regime changes as increasing quantities of runoff enter and oxygenate the flowpaths through the talus sediments. Such a process could be critical for the delivery of oxidants to the weathering environment. This pattern of $*SO_4^{2-}$ production is rather like that inferred at Midtre Lovénbreen, a polythermal Arctic glacier in schist bedrock described by Wynn et al. (2006). However, in the present study, it is the talus and perhaps the ice-marginal moraines that provide the loci for sulphide oxidation, albeit at a low rate. Similar characteristics of sulphide oxidation were also identified using these isotopes by Wadham et al's (2007) study of an Arctic glacier forefield characterised by reactive shale and carbonate lithologies. In this study, the oxidation of sulphides under conditions of anoxia was assumed to be achieved by the following reaction:

$$FeS_2 + 14Fe^{3+} + 8H_2O = 2SO_4^{2-} + 15Fe^{2+} + 16H^+ \quad (8)$$

and most likely mediated by bacteria (Bottrell and Tranter 2002). However, there exists the possibility that inorganic oxidation mechanisms still operate under anoxic conditions, such as that depicted by Eq. 9 (Schippers and Jørgensen 2001):

$$FeS_2 + 7.5MnO_2 + 11H^+ = Fe(OH)_3 + 2SO4^{2-} + 7.5Mn^{2+} + 4H_2O \quad (9)$$

Other potential oxidants, such as NO_3^- appear to be kinetically unfavourable, at least in marine sediments (Schippers and Jørgensen 2001). Whether Eq. 8 is more favourable than Eq. 9 in glacial systems is untested, but most authors invoke the former processes on the basis that the relevant microorganisms are now being detected and their kinetics are more favourable (see Hodson et al. 2008 for a review).

Microbial processes and the provision of non-snowpack N

If there are microbially mediated rock–water interactions that produce $*SO_4^{2-}$, then it is reasonable to consider the impact of microorganisms upon nitrogen export. Sustained, negative values for $*NH_4^+$ most likely indicate microbial assimilation throughout the summer, a process that has been described in Signy Island snowpacks by Hodson (2006). Hodson (2006) also described high $*NO_3^-$ concentrations in late season runoff at both Site Q2 and Site Q1, and linked this to high rock–water contact environments due to its covariance with dissolved Si. Wynn et al. (2007) used stable isotopes to show that bacteria most likely produce $*NO_3^-$ in Arctic glacial till, and so a similar analysis is reported below. Factors influencing the $\delta^{18}O$ value of NO_3^- formed by bacterial nitrification have been recently discussed elsewhere (Mayer et al. 2001; Kendall et al. 2007; Spoelstra et al. 2007). Under the simplest assumptions, autotrophic nitrification using two oxygen atoms from water and one from atmospheric O_2 would produce $*NO_3^-$ with a $\delta^{18}O_{NO_3}$ value:

$$\delta^{18}O_{NO_3} = \left(0.33 \times \delta^{18}O_{atmO_2}\right) + \left(0.66 \times \delta^{18}O_{water}\right) \quad (10)$$

As the average $\delta^{18}O_{water}$ value of waters draining from moraine and talus samples was −11.9‰, and assuming $\delta^{18}O_{atmO2} = +23.5‰$, the theoretically expected $\delta^{18}O_{NO_3}$ value for microbially produced NO_3^- for the present study is therefore −0.2‰. This value may be compared to a $\delta^{18}O_{NO_3}$ range −2.1 to +0.6‰ for samples from moraine and talus waters (corrected $\delta^{18}O_{NO_3}$ in Table 3) and +1.1 to +13.6‰ at Q2, a range which is just greater than that observed at Q1. The low values in moraine and talus waters are therefore strongly diagnostic of a microbial $*NO_3^-$ source, as are the first samples from Q2 and Q1, which show that microbial $*NO_3^-$ production was most important near the ice margin just prior to the onset of the high flow phase (i.e. Q2 values are lower than Q1 values at first; Table 3). The Tuva Glacier basin is therefore similar to the Alpine catchment described by Campbell et al. (2002), where microbial production in talus deposits is also implicated as a source of $*NO_3^-$ for runoff, and where $*NO_3^-$ can also dominate total NO_3^- during the runoff season.

However, Fig. 7 suggests that the above model of $*NO_3^-$ production is problematic. It shows the relationship between the $*NO_3^-$/total NO_3^- and $\delta^{18}O_{NO_3}$ for samples at Sites Q1, Q1, T1, T2 and M1. The negative association is significant at $p = 0.0015$ and appears to indicate a link between the importance of $*NO_3^-$ production (up to 85% of total NO_3^-) and low $\delta^{18}O_{NO_3}$ values in runoff. However, the degree of scatter in the relationship is not ideal ($r^2 = 0.69$), and the inferred $\delta^{18}O_{NO_3}$ composition for 100% snowpack NO_3^- (ie the intercept of the regression line and the x axis) is ca. +13‰, whilst the inferred $\delta^{18}O_{NO_3}$ for $*NO_3^-$ is far lower than −0.2‰ (about −8.9‰ according to the linear regression on the graph). Both end members are therefore significantly different to those expected

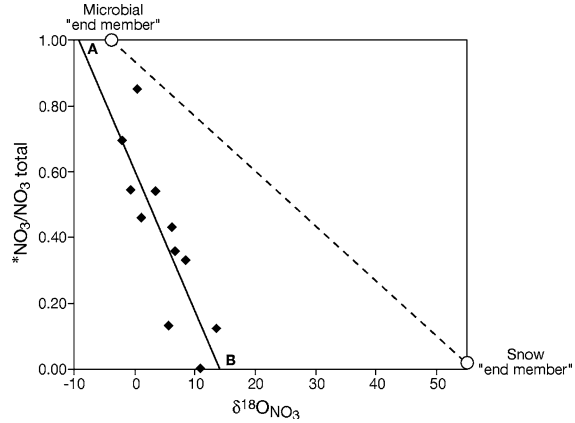

Fig. 7 The relationship between the ratio $*NO_3^-/^{total}NO_3^-$ and $\delta^{18}O_{NO_3}$. *Line* "AB" is a linear regression line through the samples. The *hatched line* marks the theoretical mixing line between NO_3 released from the snowpack and new NO_3 produced by bacteria. All data points are described in Table 3

according to our snow samples in Table 3 ($\delta^{18}O_{NO_3}$ ca. 55‰) and the theoretical microbial end member for $*NO_3^-$ (−0.2‰). Either the theoretical constraints used here are unreliable, or a major source/sink of NO_3^- has not been identified. Further studies should therefore be undertaken, ideally with a contaminant-free method for the determination of snowpack $\delta^{18}O_{NO_3}$.

A means of further investigating the biogeochemistry of nitrogen in the Tuva Glacier basin would be to consider the $\delta^{15}N_{NO_3}$ data in Table 3. However, it is likely that the main potential sources are not readily distinguishable. The range of values for the snowpack (−4.6 to +2.1‰) and the drainage waters (−2.1 to +0.4‰) are very similar to one another, and correspond to the $\delta^{15}N$ values expected for both NO_3^- in atmospheric deposition, or $*NO_3^-$ from mineralisation of organic N in pioneer environments (e.g. Campbell et al. 2002; Tye and Heaton 2007; Wynn et al. 2007). A similar problem is apparent with the $\delta^{15}N_{NH_4}$ $\delta^{15}N_{NH4}$ values in Table 3, which otherwise compare favourably to values for Arctic glacier snowpacks and meltwaters (Wynn et al. 2007) and other Signy Island samples reported by Bokhorst et al. (2007). In the latter case, values of $\delta^{15}N_{NH_4}$ in aerosol samples were +4.4 ± 4.7‰, whilst the bulk $\delta^{15}N$ of precipitation during the summer was +6.4 ± 1.1‰.

Rock weathering yields

Low yields of non-snowpack solutes are discernable in Table 1 (see also Hodson 2006). The preceding discussion suggests that this might be due to a combination of modest rates of meltwater production and the absence of a high rock–water contact environment at the glacier bed. Further, there appear to be few reactive sulphide mineral surfaces to provide efficient proton sources for acid hydrolysis (Eq. 5). Table 6 shows that the combined effect of these restrictions is to impose a system of low rates of chemical denudation relative to the worldwide selection of glacial data. Thus the present study produces a cationic denudation rate that is lower than that reported for cold-based Arctic glaciers, such as Scott Turnerbreen (see Hodgkins et al. 1997). These are some of the lowest cation yields reported in the literature, being markedly lower than those reported for carbonate lithologies, or for glaciers with large runoff fluxes through crushed bedrock in subglacial environments (Anderson et al. 1997; Hodson et al. 2000; Tranter 2005). Since both reactive lithologies (carbonates, shales and basalts) and large glaciers with subglacial weathering environments exist along the Antarctic Peninsula and its islands, it is clear that more studies of glacial chemical weathering are required before the relationship between climate warming and the production of solute fluxes can be understood here.

Conclusions

Runoff during the melt season at Tuva Glacier Basin, Signy Island clearly indicates the acquisition of solutes from crustal sources, despite the majority (58%) of solute being derived from the snowpack. We have used stable isotope and chemical tracers of rock–water interactions during the early melt season and found that solute acquisition in talus and moraine sediments is particularly important, and compensates for an absence of subglacial weathering beneath this small, cold-based glacier. The very earliest runoff conveys solute acquired from sub-oxic weathering environments in these sediments, which become more oxygenated as the melt period progresses. Evidence for NO_3^- and SO_4^{2-} production and high $p(CO_2)$ in longer residence time meltwaters was particularly pronounced in this early phase of runoff, as was the assimilation of NH_4^+. Later on, these processes are increasingly important in the glacier forefield (see also Hodson 2006). Many weathering signatures suggest that a key role is played by microbial activity within these environments, which, along with inorganic reactions, mean that the nutrients exported from the system are markedly different to those in the initial snowpack. However, low dissolved Fe concentrations (<10 μg L^{-1}) result because reactive pyrite phases are limited and the oxygenated bulk runoff stream has circum-neutral pH. Export of Fe to Fe-limited marine ecosystems will therefore almost certainly be dominated by particulate Fe_{III} phases.

While weathering environments at Tuva Glacier basin appear similar to subglacial weathering environments described elsewhere (e.g. Tranter et al. 2002), a majority of meltwaters by-pass the reactive moraine and talus sediments. The overall efficacy of solute export from crustal sources is therefore low, being ca. 163 $\Sigma*meq^+$ km^{-2} a^{-1} when expressed as a cation yield, which is dominated by Ca^{2+} and Na^+

Table 6 Catchment cationic denudation rates for a worldwide selection of glacier basins

Basin	Type	Geology	Runoff (m/a)	CDR (Σ*meq^{+}/km^{2}/a)
Broggerbreen	Arctic	Carbonate-rich	0.8–1.0	480–510
Batura Glacier	Himalayan	Carbonate-rich	2.0	1,460
Austre Broggerbreen	Arctic	Sedimentary mix	0.8–1.3	240–260
Erdmannbreen	Arctic	Sedimentary mix	0.8	190
Erikbreen	Arctic	Sedimentary mix	0.5	320
Hannabreen	Arctic	Sedimentary mix	0.8	320
Finsterwalderbreen[a]	Arctic	Shale-rich	1.1	790
Scott Turnerbreen	Arctic	Shale-rich	0.5	350
Longyearbreen[b]	Arctic	Shale-rich	0.3	322
Rieperbreen[c]	Arctic	Shale-rich	0.4	292
Tungufljot	Icelandic	Basalt	2.1	699
Hvita-S	Icelandic	Basalt	2.1	1,100
Hvita-W	Icelandic	Basalt	1.8	630
Kuannersuit[d]	Greenland	Basalt-rich	2.5	680–850
Mittivakkat[e]	Greenland	Plutonic/metamorphic	3.27	270
Midtre Lovenbreen	Arctic	Plutonic/metamorphic	1.3–1.5	450–560
Gornergletscher	Alpine	Plutonic/metamorphic	1.3	450
Tsidjiore Nouve	Alpine	Plutonic/metamorphic	1.2	510
Arolla-H	Alpine	Plutonic/metamorphic	1.7–2.3	640–685
Worthington	N American	Plutonic/metamorphic	7.7	1,600
Berendon	N American	Plutonic/metamorphic	3.7	950
S Cascade	N American	Plutonic/metamorphic	3.9	680
Chhota-Shigri	Himalayan	Plutonic/metamorphic	3.5	750
Dokriani	Himalayan	Plutonic/metamorphic	6.5	4,200
Lewis River	Arctic	Plutonic/metamorphic	0.71	94
Tuva Glacier	Antarctic	Plutonic/metamorphic	0.53	163

Data are from Hodson et al. (2000) except

[a] Wadham et al. (2001)

[b] Yde et al. 2008

[c] Hodson, unpublished data

[d] Yde et al. (2004)

[e] Yde et al. (2009)

from calcite and feldspars respectively. When compared to a global range of 94–4,200 Σ*meq^{+} km^{-2} a^{-1}, the rates of solute production and the geochemical processes responsible for them appear similar to colder Arctic glaciers.

Acknowledgments Hodson acknowledges a NERC AFI (CGS4/08) award and a National Geographic Exploration and Research Committee award for supporting his field work. Judith Brown, Simon Herniman and Bill Crowe are thanked for help with the field and lab work, whilst NERC BGS Steering Committee award (IP/776/0503) is acknowledged for the isotope support. A Leverhulme Research Fellowship is acknowledged for allowing time for Hodson to complete the manuscript, which was then improved by two anonymous reviewers.

References

Anderson SP, Drever JI, Humphrey NF (1997) Chemical weathering in glacial environments. Geology 25:399–402

Anderson SP, Drever JI, Frost CD, Holden P (2000) Chemical weathering in the foreland of a retreating glacier. Geochim Cosmochim Acta 64:1173–1189

APHA, AWWA, WEF (1995) Standard methods for examination of water and wastewater, 19th edn. American Public Health Association, New York

Bokhorst S, Huiskes A, Convey P, Aerts R (2007) External nutrient inputs into terrestrial ecosystems of the Falkland Islands and the Maritime Antarctic region. Polar Biol 30:1432–2056

Borghini F, Bargagli R (2004) Changes of major ion concentrations in melting snow and terrestrial waters from northern Victoria Land, Antarctica. Antarct Sci 16:107–115

Bottrell SH, Tranter M (2002) Sulphide oxidation under partially anoxic conditions at the bed of the Haut Glacier d'Arolla, Switzerland. Hydrol Process 16:2363–2368

Brown GH, Tranter M, And Sharp MJ (1996) Experimental investigations of the weathering of suspended sediment by alpine glacial meltwater. Hydrol Process 10:579–597

Campbell DH, Kendall C, Chang CY, Silav SR, Tonnessen KA (2002) Pathways for nitrate release from an alpine watershed: determination using $\delta^{15}N$ and $\delta^{18}O$. Water Resour Res 38(5):9-1 to 9-11

Caulkett AP, Ellis-Evans JC (1997) Chemistry of streams of Signy Island, maritime Antarctic: sources of major ions. Antarct Sci 9:3–11

Chang CCY, Langston J, Riggs M, Campbell DH, Silva SR, Kendall C (1999) A method for nitrate collection for $\delta^{15}N$ and $\delta^{18}O$ analysis from waters with low nitrate concentrations. Can J Fish Aquat Sci 56:1856–1864

Cooper RJ, Wadham JL, Tranter M, Peters N (2002) Groundwater hydrochemistry in the active layer of the proglacial zone, Finsterwalderbreen, Svalbard. J Hydrol 269:208–223

De Mora SJ, Whitehead RF, Gregory M (1991) Aqueous geochemistry of major constituents in the Alph River and tributaries in Walcott Bay, Victoria Land, Antarctica. Antarct Sci 3:73–86

Fortner SK, Tranter M, Fountain AG, Lyons B, Welch KA (2005) The geochemistry of supraglacial streams of Canada Glacier, Taylor Valley (Antarctica), and their evolution into proglacial waters. Aquat Geochem 11:391–412

Gooseff MN, McKnight DM, Lyons WB, Blum AE (2002) Weathering reactions and hyporheic exchange controls on stream water chemistry in a glacial meltwater stream in the McMurdo Dry Valleys. Water Rersour Res 38:1279. doi:10.1029/2001WR000834

Green WJ, Angle MP, Chave KE (1988) The geochemistry of Antarctic streams and their role in the evolution of four lakes of the McMurdo Dry Valleys. Geochim Cosmochim Acta 52:1265–1274

Hall KJ, Verbeek AA, Meiklejohn KI (1986) A method for the extraction and analysis of solutes from rock samples with some comments on the implications for weathering studies: an example from Signy Island, Antarctica. Br Antarct Surv Bull 70:79–84

Heaton THE, Wynn PM, Tye A (2004) Low 15N/14N ratios for nitrate in snow in the High Arctic (79°N). Atmos Environ 38:5611–5621

Hodgkins R, Tranter M, Dowdeswell JA (1997) Solute provenance, transport and denudation in a High-Arctic glacierised catchment. Hydrol Process 11:1813–1832

Hodgson DA, Roberts SJ, Bentley MJ, Smith JA, Johnson JS, Verleyen E, Vyverman W, Hodson AJ, Leng MJ, Cziferszkya A, Fox AJ, Sanderson DCW. Exploring former subglacial Hodgson Lake, Antarctica Paper I: site description, geomorphology and limnology. Quat Sci Rev. doi:10.1016/j.quascirev.2009.04.011

Hodson A (2006) Biogeochemistry of snowmelt in an Antarctic glacial ecosystem. Water Resour Res 42:W11406. doi: 10.1029/2005WR004311

Hodson A, Tranter M, Vatne G (2000) Contemporary rates of chemical denudation and atmospheric CO_2 sequestration in glacier basins: an Arctic perspective. Earth Surf Proc Land 25:1447–1471

Hodson AJ, Anesio AM, Tranter M, Fountain AG, Osborn AM, Priscu J, Laybourn-Parry J, Sattler B (2008) Glacial ecosystems. Ecol Monogr 78:41–67

Kendall C, Elliott EM, Wankel SD (2007) Tracing anthropogenic inputs of nitrogen to ecosystems. In: Michener R, Lajtha K (eds) Stable isotopes in ecology and environmental science. Blackwell, Oxford, pp 375–449

Kroopnick P, Craig H (1972) Atmospheric oxygen isotopic composition and solubility fractionation. Science 175:54–55

Lyons WB, Welch KA, Fountain AG, Dana GL, Vaughn BH, McKnight DM (2003) Surface glaciochemistry of Taylor Valley, southern Victoria Land, Antarctica and its relationship to stream chemistry. Hydrol Process 17:115–130

Mackereth FJH, Heron J, Talling JF (1978) Water analysis: some revised methods for limnologists. Freshwater Biological Association, Scientific Publication No. 36, Ambleside, UK, p 120

Mathews DH, Maling DH (1967) The geology at the South Orkney Islands: I Signy Island. Falkland Islands Dependencies Scientific Report, No. 25, 32 pp

Mayer B, Bollwerk SM, Mansfeldt T, Hutter B, Veizer J (2001) The oxygen isotope composition of nitrate generated by nitrification in acid forest floors. Geochim Cosmochim Acta 65:2743–2756

McKnight DM, Gooseff MN, Vincent WF, Peterson BJ (2008) High latitude rivers and streams. In: Vincent WF, Laybourn-Parry J (eds) Polar lakes and rivers—limnology of arctic and antarctic aquatic ecosystems, 83–102, Oxford, 327 pp

Meiklejohn KI, Hall KJ (1997) Aqueous geochemistry as an indicator of chemical on south-eastern Alexander Island. Polar Geogr 28:120–132

Mitchell A, Brown GH, Fuge R (2001) Minor and trace element export from a glacierized Alpine headwater catchment (Haut Glacier d'Arolla, Switzerland. Hydrol Process 15:3499–3524

Nezat CA, Lyons WB, Welch KA (2001) Chemical weathering in Taylor Valley streams, Antarctica. Geol Soc Am Bull 113:1401–1408

Parkhurst DL (1995) Users guide to PHREEQC—a computer programme for the speciation, reaction path, advective transport, and inverse geochemical calculations. Water Resources Investigation Report 95-4227, US Geological Survey, Lakewood, CO, 143 pp

Quayle WC, Peck LS, Peat H, Ellis-Evans JC, Harrigan PR (2002) Extreme responses to climate change in Antarctic lakes. Science 295:645

Raiswell R, Tranter M, Benning LB, Siegert M, De'ath R, Huybrechts P, Payne T (2006) Contributions from glacially derived sediment to the global iron (oxyhydr)oxide cycle: implications for iron delivery to the oceans. Geochim Cosmochim Acta 70:2765–2780

Rees CE, Jenkins WC, Monster J (1978) The sulphur isotopic composition of ocean water sulphate. Geochim Cosmochim Acta 42:377–381

Savarino J, Kaiser J, Morin S, Sigman DM, Thiemens MH (2007) Nitrogen and oxygen isotopic constraints on the origin of atmospheric nitrate in coastal Antarctica. Atmos Chem Phys 7:1925–1945

Schippers A, Jørgensen BB (2001) Oxidation of pyrite and iron sulfide by manganese dioxide in marine sediment. Geochim Cosmochim Acta 65:915–922

Sigman DM, Altabet MA, Michener R, McCorkle DC, Fry B, Holmes RM (1997) Natural abundance-level measurement of the nitrogen isotopic composition of oceanic nitrate: an adaptation of the ammonia diffusion method. Mar Chem 57:227–242

Spoelstra J, Schiff SL, Hazlett PW, Jeffries DS, Semkin RG (2007) The isotopic composition of nitrate produced from nitrification in a hardwood forest floor. Geochim Cosmochim Acta 71:3757–3771

Statham PJ, Skidmore M, Tranter M (2008) Inputs of glacially derived dissolved and colloidal iron to the coastal ocean and implications for primary productivity. Glob Biogeochem Cycles 22:GB3013. doi:10.1029/2007GB003106

Tranter M (2005) Geochemical weathering in glacial and proglacial environments. In: Drever JI (ed) Treatise on geochemistry, vol 5, 189–205. Elsevier, Amsterdam, p 605

Tranter M, Brown GH, Hodson AJ, Gurnell AM (1996) Hydrochemistry as an indicator of subglacial drainage system structure: a comparison of Alpine and sub-polar environments. Hydrol Process 10:541–556

Tranter M, Sharp MJ, Lamb H, Brown GH, Hubbard BP, Willis IC (2002) Geochemical weathering at the bed of Haut Glacier d'Arolla, Switzerland—a new model. Hydrol Process 16:959–993

Tye AM, Heaton THE (2007) Chemical and isotopic characteristics of weathering and nitrogen release in non-glacial drainage waters on Arctic tundra. Geochim Cosmochim Acta 71:4188–4205

Vincent WF, Hobbie JE, Laybourn-Parry J (2008) Introduction to the limnology of high latitude lake and river ecosystems. In: Vincent WF, Laybourn-Parry J (eds) Polar lakes and rivers—limnology of Arctic and Antarctic aquatic ecosystems, 1–23, Oxford, 327 pp

Wadham JL, Cooper RJ, Tranter M, Hodgkins R (2001) Enhancement of glacial solute fluxes in the proglacial zone of a polythermal glacier. J Glaciol 47:378–386

Wadham JL, Cooper RJ, Tranter M, Bottrell S (2007) Evidence for widspread anoxia in the proglacial zone of an Arctic glacier. Chem Geol 243:1–15

Watson AJ, Bakker DCE, Ridgwell AJ, Boyd PW, Law CS (2000) Effect of iron supply on Southern Ocean CO_2 uptake and implications for glacial atmospheric CO_2. Nature 407:730–733

Wynn PM, Hodson AJ, Heaton THE (2006) Chemical and isotopic switching within the subglacial environment of a high Arctic glacier. Biogeochemistry 78:173–193

Wynn PM, Hodson AJ, Heaton THE, Chenery SR (2007) Nitrate production beneath a High Arctic glacier, Svalbard. Chem Geol 244:88–102

Yde JC, Knudsen NT (2004) The importance of oxygen isotope provenance in relation to solute content of bulk meltwaters at Imersuaq Glacier, West Greenland. Hydrol Process 18:125–139

Yde JC, Knudsen NT, Nielsen OB (2005) Glacier hydrochemistry, solute provenance, and chemical denudation at a surge-type glacier in Kuannersuit Kuussuat, Disko Island, West Greenland. J Hydrol 300:172–187

Yde JC, Riger-Kusk M, Christiansen HH, Knudsen NT, Humlum O (2008) Hydrochemical characteristics of bulk meltwater fram an entire ablation season, Longyearbreen, Svalbard. J Glaciol 54:259–272

Yde JC, Knudsen NT, Hasholt B, Mernild SH (2009) Chemical weathering and solute provenance in a glacierised maritime catchment: Mittivakkat Gletscher, Southeast Greenland. Chem Geol (in press)